Anal. Chem. **2010,** *82,* 1349–1357

Detection of the Most Common Corneal Dystrophies Caused by *BIGH3* Gene Point Mutations Using a Multispot Gold-Capped Nanoparticle Array Chip

So Young Yoo,[†,‡] Do-Kyun Kim,[†] Tae Jung Park,[†] Eung Kweon Kim,[§] Eiichi Tamiya,[∥] and Sang Yup Lee*[,†,⊥]

BioProcess Engineering Research Center, Center for Systems & Synthetic Biotechnology, Institute for the BioCentury, Departments of Chemical & Biomolecular Engineering (BK21 program), of Bio & Brain Engineering, and of Biological Sciences, and Bioinformatics Research Center, KAIST, 335 Gwahangno, Yuseong-gu, Daejeon 305-701, Republic of Korea, Corneal Dystrophy Research Institute, Department of Ophthalmology, Severance Hospital, Yonsei University, 250 Seongsanno, Seodaemun-gu, Seoul 120-752, Republic of Korea, and Department of Applied Physics, Graduate School of Engineering, Osaka University, 2-1 Yamadaoka, Suita, Osaka 565-0871, Japan

The localized surface plasmon resonance (LSPR) optical property has recently been well employed as an effective platform for the quantitative detection of protein−protein interactions on the nanoscale. However, its advantage has not been fully explored yet in the DNA diagnosis field, especially in detecting point mutations of DNA. Point mutations of the *BIGH3* gene are associated with the most common corneal dystrophies (CDs), such as Avellino corneal dystrophy, Reis−Bucklers corneal dystrophy, and lattice corneal dystrophy. Since the detection of these corneal dystrophies is urgently needed before laser-assisted in situ keratomileusis operation to prevent blindness, genetic analysis of the *BIGH3* gene is critical in most ophthalmological clinics. In this study, we report LSPR-based detection of the *BIGH3* gene mutations by using a multispot gold-capped nanoparticle array (MG-NPA) chip. The analytical range and sensitivity of the MG-NPA chip were determined by measuring different concentrations of each CD target DNA in the range of 1 fM to 1 μM. Under the optimal conditions, the detection of DNA hybridization with each CD target DNA was performed with a detection limit of 1 pM target DNA. The selective discrimination against a single-base mismatch DNA sequence was also achieved by using both homozygous and heterozygous CD samples. It demonstrates that the label-free LSPR-based optical biosensor system employing the MG-NPA chip provides a new diagnostic platform allowing the selective and sensitive detection of various DNA point mutations, leading to possible diagnosis of mutation-related diseases including corneal dystrophies reported here.

Mutations in the human transforming growth factor β induced (*BIGH3*; OMIM 601692) gene on chromosome 5q31 are responsible for autosomal dominant corneal dystrophies, including Avellino corneal dystrophy (ACD; OMIM 607541), Reis−Bucklers corneal dystrophy (RBCD; OMIM 121900), and lattice corneal dystrophy (LCD; OMIM 122200).[1−3] The genotype of each corneal dystrophy (CD) was characterized as follows: 418G → A (ACD), 418G → T (RBCD), and 417C → T (LCD).[4] These single mutations cause amino acid substitutions in the BIGH3 protein (Table 1). The importance of ACD diagnosis before keratectomy has received great attention in recent reports,[5,6] which suggested that molecular genetic analysis of *BIGH3* gene mutation is suitable for the diagnosis of an atypical or ambiguous corneal appearance.

Rapid advances in the development of highly selective and sensitive biological detection methods, such as real-time PCR and biochip technologies, over the past two decades, have greatly facilitated medical diagnosis, mostly utilizing fluorescent or colorimetric dye as an indicator for the presence of specific protein

* To whom correspondence should be addressed. Phone: +82-42-350-3930. Fax: +82-42-350-8800. E-mail: leesy@kaist.ac.kr.

† BioProcess Engineering Research Center, Center for Systems & Synthetic Biotechnology, and Institute for the BioCentury, KAIST.

‡ Current address: Department of Bioengineering, University of California, Berkeley, California 94720.

§ Yonsei University.

∥ Osaka University.

⊥ Departments of Chemical & Biomolecular Engineering, of Brain & Bioengineering, and of Biological Sciences and Bioinformatics Research Center, KAIST.

(1) Afshari, N. A.; Mullally, J. E.; Afshari, M. A.; Steinert, R. F.; Adamis, A. P.; Azar, D. T.; Talamo, J. H.; Dohlman, C. H.; Dryja, T. P. *Arch. Ophthalmol. (Chicago)* **2001**, *119*, 16–22.

(2) Stone, E. M.; Mathers, W. D.; Rosenwasser, G. O. D.; Holland, E. J.; Folberg, R.; Krachmer, J. H.; Nichols, B. E.; Gorevic, P. D.; Taylor, C. M.; Streb, L. M.; Fishbaugh, J. A.; Daley, T. E.; Sucheski, B. M.; Sheffield, V. C. *Nat. Genet.* **1994**, *6*, 47–51.

(3) Munier, F. L.; Korvatska, E.; DjemaiÃ, A.; Paslier, D. L.; Zografos, L.; Pescia, G.; Schorderet, D. F. *Nat. Genet.* **1997**, *15*, 247–251.

(4) Munier, F. L.; Frueh, B. E.; Othenin-Girard, P.; Uffer, S.; Cousin, P.; Wang, M. X.; Héon, E.; Black, G. C. M.; Blasi, M. A.; Balestrazzi, E.; Lorenz, B.; Escoto, R.; Barraquer, R.; Hoeltzenbein, M.; Gloor, B.; Fossarello, M.; Singh, A. D.; Arsenijevic, Y.; Zografos, L.; Schorderet, D. F. *Invest. Ophthalmol. Vis. Sci.* **2002**, *43*, 949–954.

(5) Wan, X. H.; Lee, H. C.; Stulting, R. D.; Kim, T.; Jung, S. E.; Kim, M. J.; Kim, E. K. *Cornea* **2002**, *21*, 223–226.

(6) Jun, R. M.; Tchah, H.; Kim, T.-I.; Stulting, R. D.; Jung, S. E.; Seo, K. Y.; Lee, D. H.; Kim, E. K. *Ophthalmology* **2004**, *111*, 463–468.

10.1021/ac902410z
Published on Web 01/21/2010

and/or DNA interactions.[1−7] Recently, a DNA chip has been developed for diagnosing different types of corneal dystrophies by detecting multiple genotypes simultaneously, and it has proven to be a simple and reliable diagnostic method.[8] However, most conventional diagnostic systems require a relatively long assay time that involves troublesome liquid-handling and labeling procedures and the use of expensive reagents and instruments. Thus, there has been great interest in developing a label-free diagnostic system to monitor biomolecular interactions easily in a short assay time.[9] In particular, label-free optical methods for detecting biological interactions enable monitoring the biomolecular interactions in real time and improve the reliability of the results using a fewer step procedure.[10−13]

Localized surface plasmon resonance (LSPR) has been considered as a useful optical property for medical applications because it measures the local refractive index, which changes with the composition, size, shape, and local electric environments.[14,15] This method detects an immediate increase in the thickness of a biomolecular layer on the surface of a sensitive element caused by a reaction between the biomolecule in the solution and the receptor layer immobilized on the surface. LSPR-based optical biosensors usually use noble-metal nanoparticles such as gold, silver, and platinum. Recently, a number of studies on the label-free LSPR-based biosensor and related techniques based on the light absorption of the nanostructures have been reported.[16−24] Recently, we reported the development of a gold-capped nanoparticle array chip, which is made by the monolayer formation of surface-adsorbed silica spheres, followed by the deposition of a thin gold layer on their surface.[25,26] The gold-capped nanoparticle array chip brings several advantages along with its cost-effective and easy fabrication procedure. In addition, the optical characteristics of the gold-capped nanoparticle array chip depend on the diameter of the dielectric nanoparticle and the thickness of the gold layer, which can be controlled for intended uses. This LSPR-based biochip has demonstrated its linear dependence on the refractive index of the surrounding environment. The shift to longer wavelength and the change in extinction intensity were observed by the biomolecular adsorption on the gold surface in the devices.

Several biosensing applications of surface plasmon resonance have been examined for detecting DNA−DNA hybridization as well as detecting protein−protein interaction such as antigen−antibody reactions.[27] Colloidal aggregation assay was performed for the detection of the aggregation of gold colloids upon DNA−DNA hybridization.[28,29] By changing the temperature and analyzing the melting temperature, DNA−DNA affinity could be analyzed.[30] In these studies, it was possible to detect the complementary vs noncomplementary DNAs under various conditions. However, detection of single point mutations has not been attempted. Here, we report the development of a label-free LSPR-based optical biosensor system for rapid, sensitive, and quantitative detection of DNA point mutations. Three kinds of point mutations in the *BIGH3* gene, an important genetic disease causing corneal dystrophies, were detected simultaneously using a 20-multispot gold-capped nanoparticle array (MG-NPA) chip.

EXPERIMENTAL SECTION

DNA Cloning and Sequence Analysis. Polymerase chain reaction (PCR) experiments were performed with a PCR thermal cycler (BioMetra, Gottingen, Germany) using a high-fidelity PCR system (Boehringer Mannheim, Mannheim, Germany). Restriction enzymes and DNA-modifying enzymes were purchased from New England Biolabs (Berverly, MA). The exon 4 regions of the *BIGH3* genes for normal, ACD, RBCD, and LCD types were obtained by PCR amplification using the primers *Xho*I-ori4Fw (5′-GGTCAGCTCGAGCCCCAGAGGCCATCCCTCCT-3′) and *Sac*II-ori4Re (5′- GGTCAGCCGCGGCCGGGCAGACGGAGGTCATC-3′) listed in Table 2 and the genomic DNA of blood samples from participants as templates. Then the PCR products of normal, ACD, RBCD, and LCD (249 bp) types were digested with *Xho*I and *Sac*II and ligated into the same sites of pBluescript II SK(−) (3.0 kb; Stratagene, La Jolla, CA) to construct pBIGH3-NLe4, pBIGH3-ACDe4, pBIGH3-RBCDIe4, and pBIGH3-LCDIe4, respectively. *Escherichia coli* TOP10 (*F- mcrA Δ(mrr-hsdRMS-mcrBC) φ80lacZΔM15 ΔlacX74 nupG recA1 araD139 Δ(ara-leu)7697 galE15 galK16 rpsL(Str^R) endA1 λ$^-$*; Invitrogen, Carlsbad, CA) was used as a cloning host. For the verification of mutations and the identification of the mutation types and the cloned sequences, DNA sequences of all clones were confirmed by sequencing using an automatic DNA sequencer (ABI Prism 377, Applied Biosystems, Foster, CA).

Preparation of Target DNA. To prepare the target DNA, asymmetric PCR was carried out in a 50 μL reaction mixture

(7) Yoshida, S.; Yamaji, Y.; Yoshida, A.; Noda, Y.; Kumano, Y.; Ishibashi, T. *Hum. Genet.* **2005**, *116*, 518–524.
(8) Yoo, S. Y.; Kim, T.-I.; Lee, S. Y.; Kim, E. K.; Keum, K. C.; Yoo, N. C.; Yoo, W. M. *Br. J. Ophthalmol.* **2007**, *91*, 722–727.
(9) Taylor, C. J.; Bain, L. A.; Richardson, D. J.; Spiro, S.; Russell, D. A. *Anal. Biochem.* **2004**, *328*, 60–66.
(10) Su, X.; Zhang, J. *Sens. Actuators, B* **2004**, *100*, 309–314.
(11) Osmond, R. I. W.; Kett, W. C.; Skett, S. E.; Coombe, D. R. *Anal. Biochem.* **2002**, *310*, 199–207.
(12) Nath, N.; Chilkoti, A. *Anal. Chem.* **2004**, *76*, 5370–5378.
(13) Haake, H.-M.; Schütz, A.; Gauglitz, G.; Fresen, J. *Anal. Chem.* **2000**, *366*, 576–585.
(14) Haes, A. J.; Van Duyne, R. P. *J. Am. Chem. Soc.* **2002**, *124*, 10596–10604.
(15) Haes, A. J.; Zou, S.; Schatz, G. C.; Van Duyne, R. P. *J. Phys. Chem. B* **2004**, *108*, 6961–6968.
(16) Jain, P. K.; Qian, W.; El-Sayed, M. A. *J. Am. Chem. Soc.* **2006**, *128*, 2426–2433.
(17) Pierrat, S.; Zins, I.; Breivogel, A.; Sönnichsen, C. *Nano Lett.* **2007**, *7*, 259–263.
(18) Skewis, L. R.; Reinhard, B. M. *Nano Lett.* **2008**, *8*, 214–220.
(19) Wang, Y.; Qian, W.; Tan, Y.; Ding, S. *Biosens. Bioelectron.* **2008**, *23*, 1166–1170.
(20) Dahlin, A. B.; Tegenfeldt, J. O.; Höök, F. *Anal. Chem.* **2006**, *78*, 4416–4423.
(21) Marinakos, S. M.; Chen, S.; Chilkoti, A. *Anal. Chem.* **2007**, *79*, 5278–5283.
(22) Mayer, K. M.; Lee, S.; Liao, H.; Rostro, B. C.; Fuentes, A.; Scully, P. T.; Nehl, C. L.; Hafner, J. H. *ACS Nano* **2008**, *2*, 687–692.
(23) Huang, H.; He, C.; Zeng, Y.; Xia, X.; Yu, X.; Yi, P.; Chen, Z. *Biosens. Bioelectron.* **2009**, *24*, 2255–2259.
(24) Kim, D.-K.; Kerman, K.; Hiep, H. M.; Saito, M.; Yamamura, S.; Takamura, Y.; Kwon, Y.-S.; Tamiya, E. *Anal. Biochem.* **2008**, *379*, 1–7.
(25) Endo, T.; Kerman, K.; Nagatani, N.; Tamiya, E. *J. Phys.: Condens. Matter* **2007**, *19*, 215201.
(26) Endo, T.; Yamamura, S.; Kerman, K.; Tamiya, E. *Anal. Chim. Acta* **2008**, *614*, 182–189.
(27) Sepulveda, B.; Angelome, P. C.; Lechuga, L. M.; Liz-Marzan, L. M. *Nanotoday* **2009**, *4*, 244–251.
(28) Elghanian, R.; Storhoff, J. J.; Mucic, R. C.; Letsinger, R. L.; Mirkin, C. A. *Science* **1997**, *277*, 1078–1081.
(29) Alivisatos, A. P.; Johnsson, K. P.; Peng, X.; Wilson, T. E.; Loweth, C. J.; Bruchez, M. P., Jr.; Schultz, P. G. *Nature* **1996**, *382*, 609–611.
(30) Sönnichsen, C.; Reinhard, B. M.; Liphardt, J.; Alivisatos, A. P. *Nat. Biotechnol.* **2005**, *23*, 741–745.

Table 1. Single Mutations in *BIGH3* Associated with the Most Common Corneal Distrophies

sequence (5′ to 3′) (mutation position)	mutation	phenotype	exon no.	target sequence motif (5′ to 3′ sequence of exon 4)
C**G**C to C**A**C (418)	R124H	Avellino corneal dystrophy (ACD)	4	CCCTACCACTCTCAAACCTTTACGAGACCCTGGGAGTCGT TGGATCCACCACCACTCAGCTGTACACGGAC**A**CACGGAGA AGCTGAGGCCTGAGATGGAGGGGCCCGGCAGCTTCACCATC TTCGCCCCTAGCAACGAGGCCTGGGCCTCCTTGCCAGCT
C**G**C to C**T**C (418)	R124L	Reis−Bucklers corneal dystrophy (RBCD)	4	CCCTACCACTCTCAAACCTTTACGAGACCCTGGGAGTCGT TGGATCCACCACCACTCAGCTGTACACGGAC**T**CACGGAGA AGCTGAGGCCTGAGATGGAGGGGCCCGGCAGCTTCACCATC TTCGCCCCTAGCAACGAGGCCTGGGCCTCCTTGCCAGCT
CGC to **T**GC (417)	R124C	lattice corneal dystrophy (LCD)	4	CCCTACCACTCTCAAACCTTTACGAGACCCTGGGAGTCGT TGGATCCACCACCACTCAGCTGTACACGGAC**T**GCACGGAGA AGCTGAGGCCTGAGATGGAGGGGCCCGGCAGCTTCACCATC TTCGCCCCTAGCAACGAGGCCTGGGCCTCCTTGCCAGCT

Table 2. DNA Oligonucleotides Used in This Study

category	name	length (mer)	sequence (5′ to 3′)	region/ mutation	purpose	ref
primers	*Xho*I-ori4Fw[a]	32	GGTCAGCTCGAGCCCCAGAGGCCATCCCTCCT	exon 4	cloning	this study
	*Sac*II-ori4Re[a]	32	GGTCAGCCGCGGCCGGGCAGACGGAGGTCATC	exon 4	cloning	this study
	Exon4Fw	20	AGCCCTACCACTCTCAAACC	exon 4	target PCR	8
	Exon4Re	18	CAGGCCTCGTTGCTAGGG	exon 4	target PCR	8
	Ori4Fw	20	CCCCAGAGGCCATCCCTCCT	exon 4	target PCR	8
	Exon4Fw2	20	TGCAGCCCTACCACTCTCAA	exon 4	target PCR	this study
	50Fw	18	CCACCACCACTCAGCTGT	exon 4	target PCR	this study
	100Re	18	CTCAGGCCTCAGCTTCTC	exon 4	target PCR	this study
	Ori4Re	20	CCGGGCAGACGGAGGTCATC	exon 4	target PCR	8
probes	4-CGC	15	ACGGACCGCACGGAG	R124	normal	8
	4-CAC[b]	15	ACGGACC**A**CACGGAG	R124H	ACD	8
	4-CTC[b]	15	ACGGACC**T**CACGGAG	R124L	RBCD	8
	4-TGC[b]	15	CACGGAC**T**GCACGGA	R124C	LCD	8
target DNAs[c]	comNLe4-30	30	TCAGCTTCTCCGTGCGGTCCGTGTACAGCT	exon 4	normal	this study
	comACD-30	30	TCAGCTTCTCCGTG**T**GGTCCGTGTACAGCT	exon 4	ACD	this study
	comRBCD-30	30	TCAGCTTCTCCGTG**A**GGTCCGTGTACAGCT	exon 4	RBCD	this study
	comLCD-30	30	TCAGCTTCTCCGTG**C**AGTCCGTGTACAGCT	exon 4	LCD	this study
	comNLe4-50	50	CTCAGGCCTCAGCTTCTCCGTGCGGTCCGT GTACAGCTGAGTGGTGGTGG	exon 4	normal	this study
	comNLe4-100	100	CTCAGGCCTCAGCTTCTCCGTGCGGTCCGT GTACAGCTGAGTGGTGGTGGATCCAACGACTCCCA GGGTCTCGTAAAGGTTTGAGAGTGGTAGGGCTGCA	exon 4	normal	this study
	comNLe4-147	147	CAGGCCTCGTTGCTAGGGGCGAAGATGGTGAAGCT GCCGGGCCCCTCCATCTCAGGCCTCAGCTTCTCCG TGCGGTCCGTGTACAGCTGAGTGGTGGTGGATCCA ACGACTCCCAGGGTCTCGTAAAGG TTTGAGAGTGGTAGGGCT	exon 4	normal	this study
	comNLe4-190	190	CCGGGCAGACGGAGGTCATCTCACAGCTGGCAAGGAGGCCCAGGCC TCGTTGCTAGGGGCGAAGATGGTGAAGCTGCCGGGCC CCTCCATCTCAGGCCTCAGCTTCTCCGTGCGGTCCGT GTACAGCTGAGTGGTGGTGGATCCAACGACTCC CAGGGTCTCGTAAAGGTTTGAGAGTGGTAGGGCTGCA	exon 4	normal	this study
	comNLe4-225	225	CCGGGCAGACGGAGGTCATCTCACAGCTGGCAAGGAGGCCCAGGCCT CGTTGCTAGGGGCGAAGATGGTGAAGCTGCCGGGCCCCTC CATCTCAGGCCTCAGCTTCTCCGTGCGGTCCGT GTACAGCTGAGTGGTGGTGGATCCAACG ACTCCCAGGGTCTCGTAAAGGTTTGAGAGTGGTAGGGCTGC AGGAGCAGAAGACAGAAGGAGGGATGGCCTCTGGGG	exon 4	normal	this study

[a] Restriction enzyme sites are underlined. [b] The point mutation sequences are shown in bold. [c] The target DNA sequences are reverse complementary to the corresponding target sequence. Underlines represent the region of hybridization with the probe DNA. For the target sequences longer than 50-mer, the mutant sequences are not shown.

containing 1× buffer, 0.2 mM dNTP, 1 U of Taq polymerase (Takara Shuzo, Shiga, Japan), one of four different cloned DNA templates (normal, ACD, RBCD, or LCD type), and the forward and backward primers listed in Table 2. For preparing different target DNAs having different sizes of 30−225-mer, 50-, 100-, 147-, 190-, and 225-mer target DNAs were amplified by PCR using primer sets (Table 2) of 3 μM 50Fw and 30 μM 100Re, 3 μM Exon4Fw2 and 30 μM 100Re, 3 μM Exon4Fw2 and 30 μM Exon4Re, 3 μM Exon4Fw2 and 30 μM Ori4Re, and 3 μM Ori4Fw and 30 μM Ori4Re, respectively. The 30-mer targets were synthesized (comNLe4-30, comACD-30, comRBCD-30, comLCD-30; Table 2). To apply patients' DNA onto this system, DNAs were extracted using the JETQUICK blood and cell culture DNA spin kit (GENOMED GmbH, Löhne, Germany) from the peripheral blood of participants who provided their informed consent before the tests and used as template DNAs for the PCR reaction. The amplified target products were directly added to the hybridization solution containing 6× SSPE (0.9 M NaCl, 10 mM $NaH_2PO_4 \cdot H_2O$, 1 mM EDTA, pH 7.4) and 20% (v/v) formamide (Figure 1).

Fabrication of the MG-NPA Chip. Figure 2A shows the MG-NPA chip and the associated equipment. Slide glass substrates

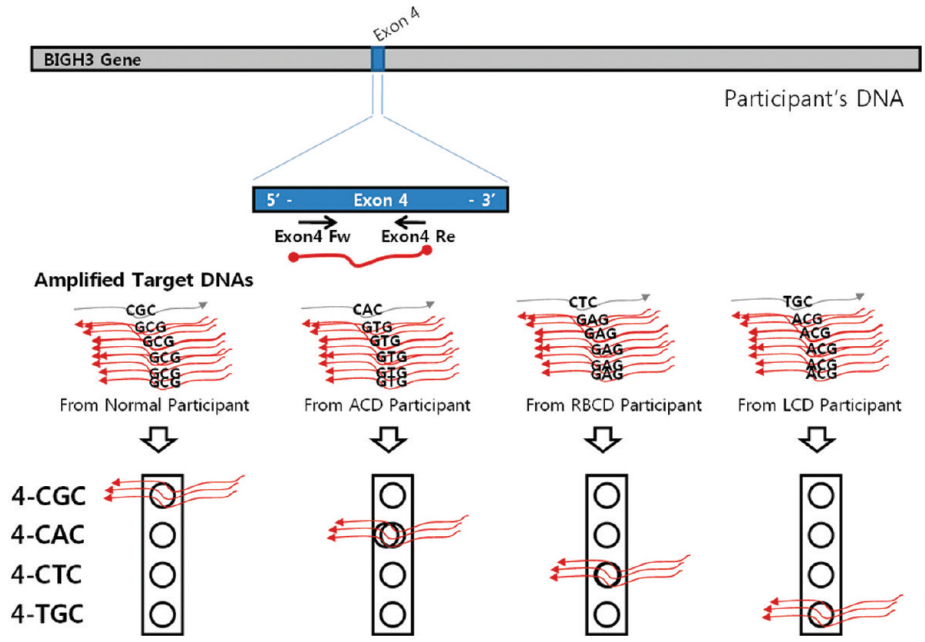

Figure 1. Mutations causing ACD, RBCD, and LCD and their point mutations compared with the normal gene. The schemes for PCR amplification of the target DNA and hybridization on the MG-NPA chip are also shown.

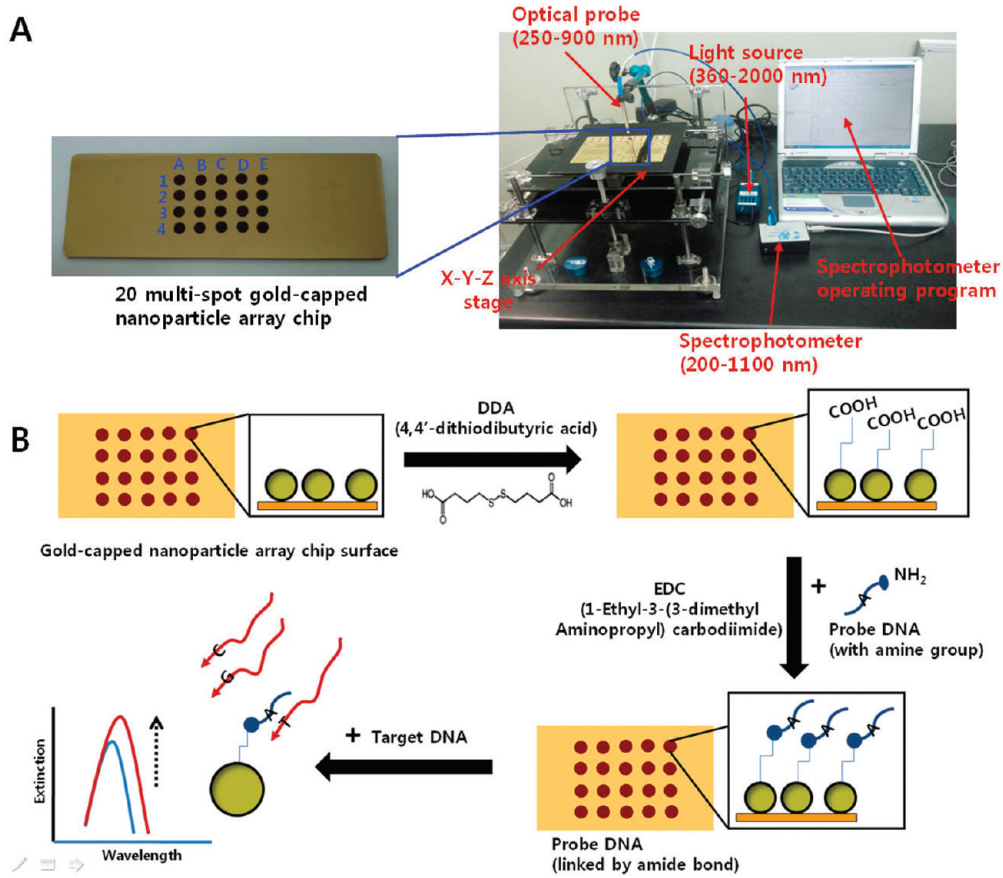

Figure 2. MG-NPA chip system for the label-free detection of DNA point mutations. (A) Experimental setup and the system for the label-free LSPR-based MG-NPA chip. The diameter of one spot is 2 mm. (B) Schematic illustration of probe DNA immobilization on the chip, target DNA hybridization, and label-free optical detection.

(S-1215, 76 mm × 26 mm × 1 mm, Matsunami Glass Ind., Osaka, Japan) were cleaned thoroughly by ultrasonication for 10 min in acetone, ethanol, and ultrapure water, respectively. For deposition of chromium and gold on the slide glass substrate, an E-beam evaporator (MHS 1800, MooHan, Korea) was used at a base pressure of 4×10^{-6} Torr. A bottom Cr layer of 5 nm in height and Au layer of 40 nm in height were deposited onto the slide glass subsequently. The growth rates were manually adjusted

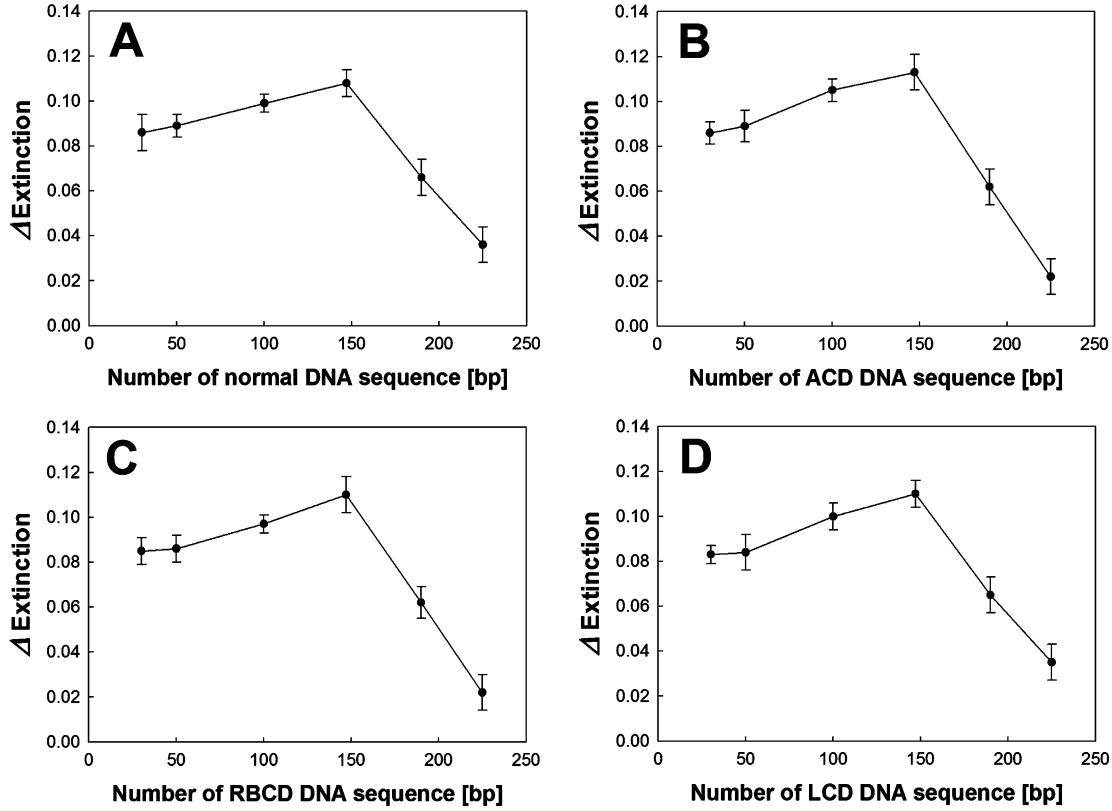

Figure 3. Spectrum profiles obtained with the target DNA samples of different lengths on the MG-NPA chip. The hybridization signal became stronger with longer target DNA up to 147-mer and then became lower with 190- and 225-mer target DNAs. Target DNAs applied are (A) normal (normal *BIGH3* gene sequence without mutation), (B) ACD, (C) RBCD, and (D) LCD.

to 0.1 Å/s and monitored with a thickness monitor (model TM-350, MAXTEK, Santa Fe Springs, CA). The surfaces of silica nanoparticles (100 nm in diameter) were modified using 1% (v/v) (3-aminopropyl)triethoxysilane (γ-APTES; Sigma-Aldrich, St. Louis, MO) solution in ethanol with stirring at room temperature. Then the suspension was centrifuged at 3500 rpm for 5 min and the supernatant discarded. The amino-surface-modified silica nanoparticles were washed with ultrapure water three times to remove residual solution. The nanoparticles were then dried at 120 °C for 10 min in an oven and stored in a desiccator. Just before use, the silica nanoparticle solution was prepared at 1% (w/v) by dispersion in ultrapure water. For the fabrication of the MG-NPA chip, a 20-multispot (diameter of 2 mm) silicon-rubber mask was carefully placed on the surface of the Cr/Au-deposited slide glass. Then 1 mM 4,4′-dithiodibutyric acid (DDA; Sigma-Aldrich) was introduced to the gold-layered surface and left for 1 h to allow formation of a self-assembled monolayer (SAM) of the DDA. The surface-activated silica nanoparticles and 400 mM 1-ethyl-3-[3-(dimethylamino)-propyl]carbodiimide (EDC; Sigma-Aldrich) were mixed at 1:1 and introduced to the activated SAM formation for 1 h. The EDC was used to serve activation of a carboxyl group of SAM formation, which, in turn, formed esters with the amino group of the nanoparticles. After addition of each solution, the nanoparticle-layered substrates were rinsed thoroughly with ultrapure water to remove the excess surface-modified nanoparticles and then dried at room temperature. Finally, a top Au layer 30 nm in height was deposited onto the nanoparticle-layered substrate using the E-beam evaporator.

Immobilization of Probe DNA on the MG-NPA Chip. The 3′-termini of the DNA probes (Table 2) were modified with amine residues using an amino-linker column (Cruachem, Glasgow, Scotland) for their immobilization on the MG-NPA chip. Immobilization of the 15-mer probes onto the 20-MG-NPA chip surface was carried out as shown in Figure 2B. DDA (1 mM) was introduced to the nanoparticle surface for the SAM formation in 1 h. The SAM was functionalized with 400 mM EDC for 1 h, and the probe DNAs (10 μM) with amino groups were immobilized by forming amide bonds with activated carboxyl groups of the SAM on the surface for 2 h.

Optical Biosensor System. The instruments for the evaluation of the optical properties on the MG-NPA chip were based on an LSPR spectroscopy microscopy system (Ocean Optics, Dunedin, FL). The experimental setup for the evaluation of optical properties is shown in Figure 2A. The optical system was equipped with a tungsten halogen light source (LS-1, wavelength range of 360−2000 nm), a spectrophotometer (USB40000 UV−vis, wavelength range of 200−1100 nm), and an optical fiber probe bundle (R-200-7 UV−vis, fiber core diameter of 300 μm, wavelength range of 250−900 nm). White light emerging from the optical fiber bundle was incident onto the MG-NPA chip from the vertical direction. The reflected light was coupled into the detection fiber probe in the same bundle and analyzed using the UV−vis spectrophotometer linked to the bundle. All spectra were taken in the range of 450−750 nm in air at room temperature.

Label-Free Detection of DNA Hybridization. The surfaces of the MG-NPA chip, onto which DNA probes were immobilized, were rinsed thoroughly with ultrapure water and dried at room

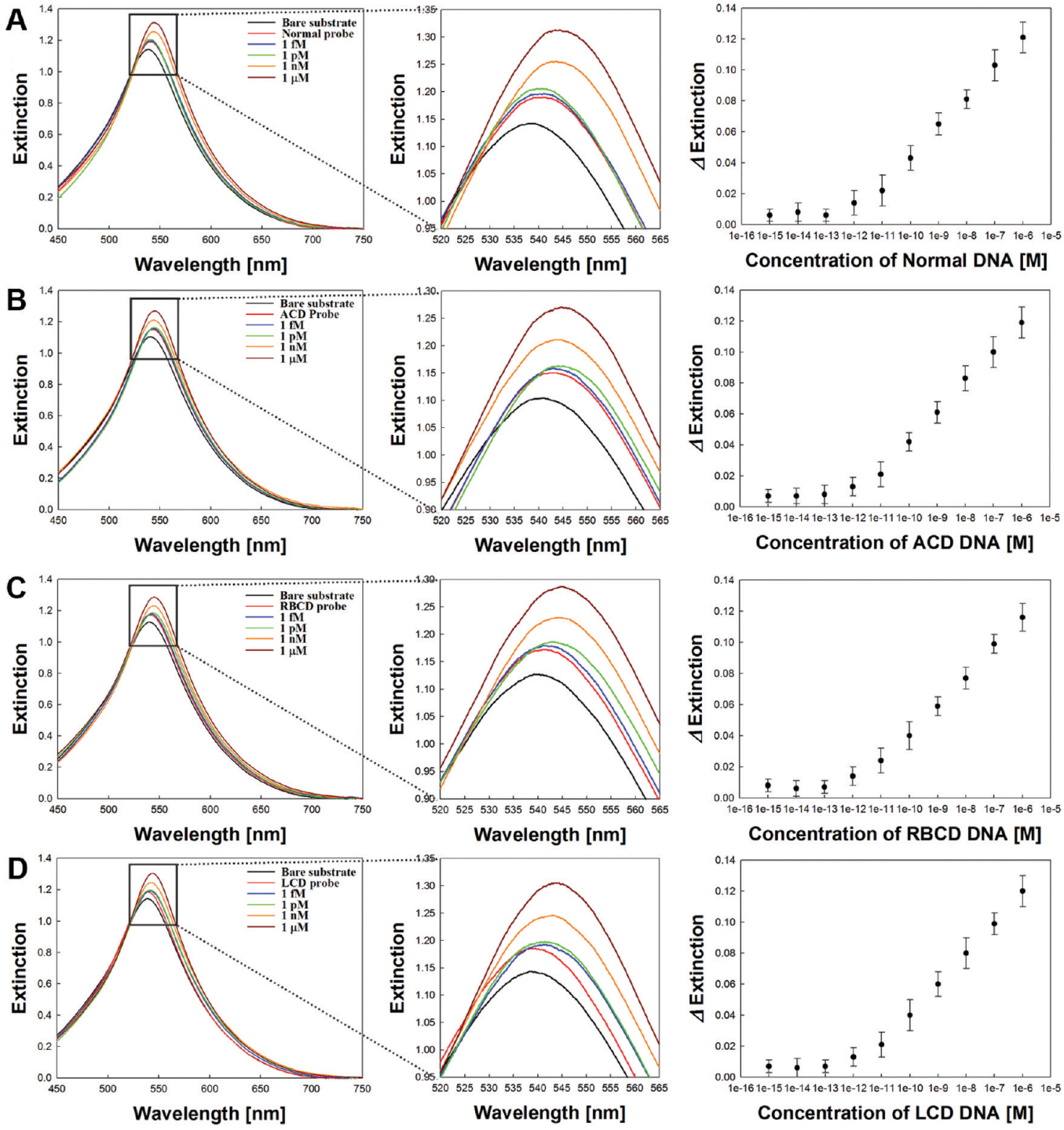

Figure 4. Superimposed extinction spectrum curves and calibration plots obtained after hybridization of four target DNAs representing (A) normal (normal *BIGH3* gene sequence without mutation), (B) ACD, (C) RBCD, and (D) LCD types with four corresponding probe DNAs immobilized on the surface of the MG-NPA chip. The concentration of the target DNA was varied from 1 fM to 1 μM. As the concentration of target DNA increased, the extinction also increased.

temperature. A desired concentration of target DNA was introduced to the probe DNA immobilized MG-NPA chip surface, and the hybridization reaction was performed by incubating for 6 h in a humidified condition at room temperature. After a stringent washing of the surface with ultrapure water, the spectrum change was monitored by using the optical biosensor system. Each assay was performed on a new chip.

RESULTS AND DISCUSSION

System Design for the Detection of the DNA Point Mutation. As the sequences of numerous genes related to genetic diseases are becoming available, it becomes increasingly important to diagnose them at their early stages. A single point mutation in the *BIGH3* gene can cause inevitable visual loss after laser-assisted in situ keratomileusis (LASIK) operation, which often happens in

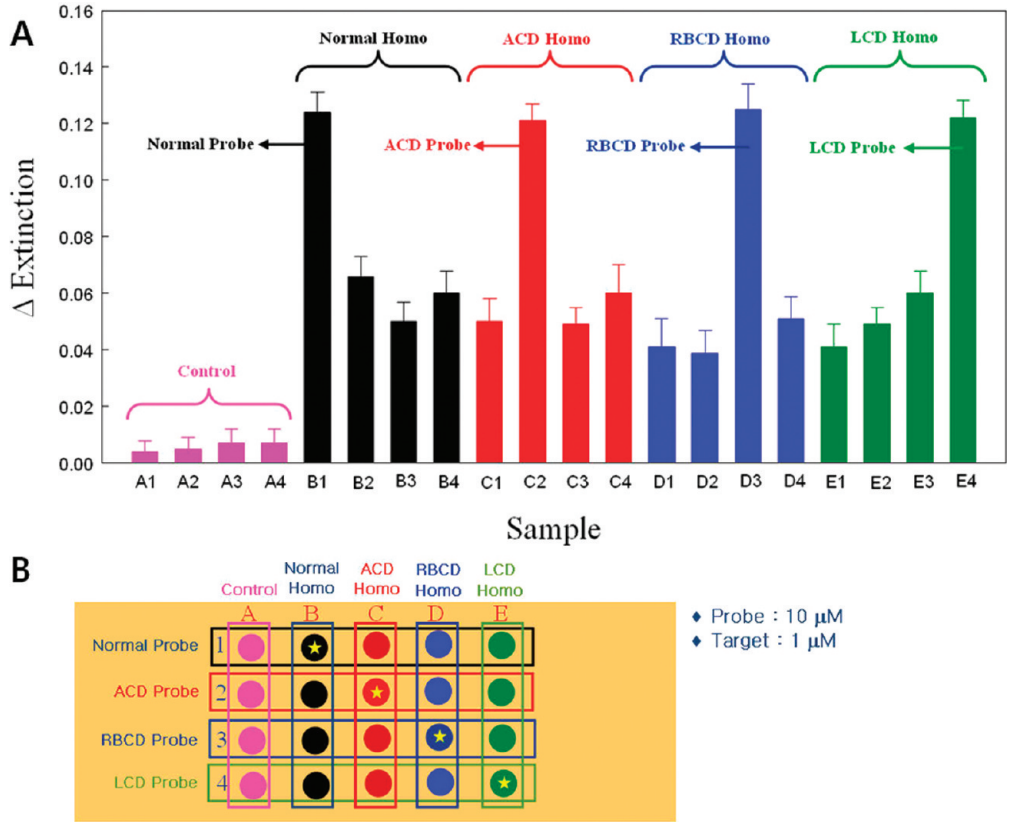

Figure 5. Affinity stringency observed from the hybridization of homozygous target DNAs with the probe DNAs using the 20-MG-NPA chip. (A) Extinction change at each spot showing affinity stringency. (B) Design of the 20-MG-NPA chip. Each probe DNA was immobilized at the 1−4 positions, and different target DNA samples were applied onto the B−E positions. Hybridization buffer without DNA sample was applied onto the A position as a negative control. The asterisks at positions B1, C2, D3, and E4 represent the positions of perfect match sequences between each type of probe DNA and each homozygous CD sample.

the cases of heterozygous ACD patients with ambiguous symptoms. In previous studies, the genetic analyses were successfully performed by fluorescence-based technologies, such as DNA sequencing, real-time PCR, and the DNA chip.[1−8] In this study, we attempted to use a label-free optical biosensor system based on LSPR optical properties. The optical properties of the LSPR-based biosensor using noble-metal nanoparticles brought about the red shift in the wavelength and the increment of the extinction intensity.[31] Hence, this system incorporates the advantages of both DNA chip technology and multiple LSPR-based nanoparticle array chip technology. Using the MG-NPA chip developed in this study, the optical characteristics can be obtained more efficiently than when using conventional biochips. The conventional LSPR-based nanochips involve complicated procedures during the synthesis and immobilization of uniformly sized metal nanoparticles. However, the MG-NPA chip is easy to fabricate via the self-assembly of surface-functionalized nanoparticles and the subsequent gold deposition onto them. The optical characteristics, such as the extinction intensity and the peak wavelength in our MG-NPA chip, are influenced by the probe−target affinity. The 15-mer specific probes (Table 2), which were confirmed to detect single point mutations in the *BIGH3* genes,[8] were immobilized by an amide bond on the MG-NPA chip surface. All target DNAs were amplified and applied onto the MG-NPA chip, and their hybridization signals were analyzed by the label-free LSPR-based optical biosensor system as shown in Figure 2. Each probe was dispensed onto the predetermined spot position which was separated with a pitch of 2 mm interval to prevent cross-contamination. LSPR spectra were measured after incubation with the target DNA samples at room temperature for 6 h. The extinction intensity change showed their binding affinity. The surface coverage of nanoparticles was determined from the SEM image of the MG-NPA chip surface (see the Supporting Information, Figure S1). The number of immobilized DNA molecules on the spot of the MG-NPA chip was calculated following the method reported previously,[32] and the results are shown in Table S1 in the Supporting Information.

Hybridization with Target DNAs Differing in Length. Figure 3 shows the spectrum profiles when target DNA samples of different lengths were applied onto the MG-NPA chip. The stability of DNA hybrids between the target DNAs and the short DNA probes on the chip depends on several parameters, such as the nucleic acid length, base composition, concentrations of the probe and target DNAs, spacer length, hybridization temperature and time, labeling dyes, and ionic strength,[33] which have to be optimized. The effects of the target DNA length on the efficiency of hybridization were tested with six different target DNAs (30-, 50-, 100-, 147-, 190-, and 225-mer). The hybridization signal became

(31) Anker, J. N.; Paige Hall, W.; Lyandres, O.; Shah, N. C.; Zhao, J.; Van Dyune, R. P. *Nat. Mater.* **2008**, *7*, 442–453.
(32) Stakenborg, T.; Peeters, S.; Reekmans, G.; Laureyn, W.; Jans, H.; Borghs, G.; Imberechts, H. *J. Nanopart. Res.* **2008**, *10*, 143–152.
(33) Conner, B. J.; Reyes, A. A.; Morin, C.; Itakura, K.; Teplitz, R. L.; Wallace, R. B. *Proc. Natl. Acad. Sci. U.S.A.* **1983**, *80*, 278–282.

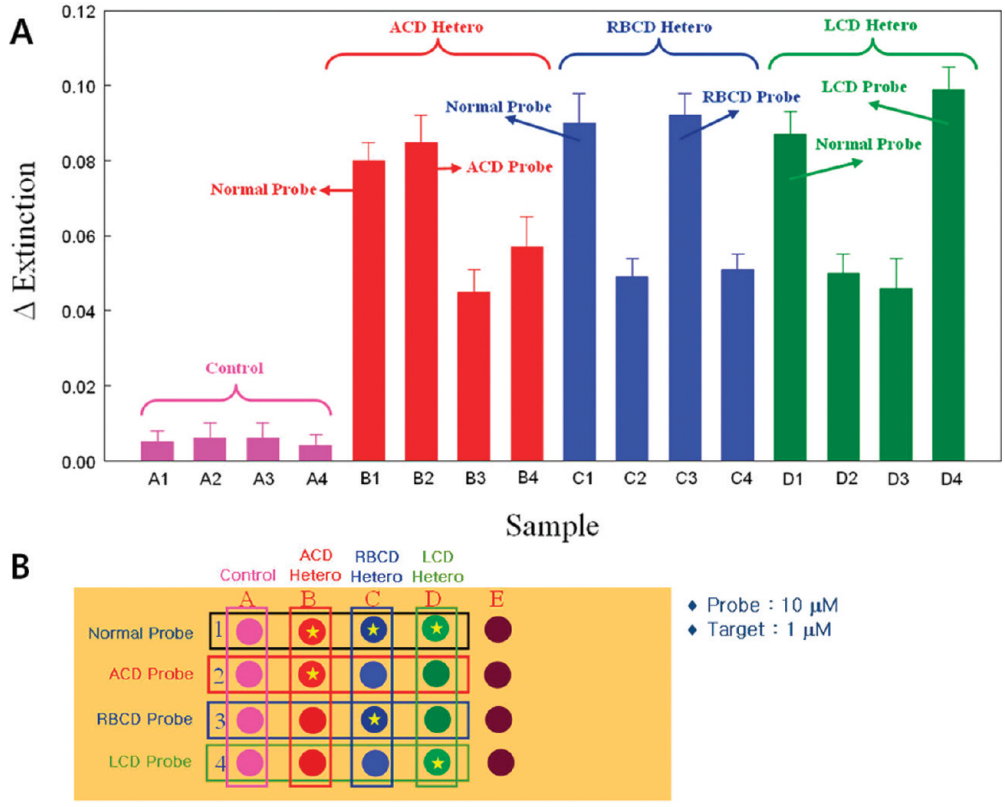

Figure 6. Affinity stringency observed from the hybridization of heterozygous target DNAs amplified from CD patients with the probe DNAs using the 20-MG-NPA chip. (A) Extinction change at each spot showing affinity stringency. (B) Design of the 20-MG-NPA chip. Each probe DNA was immobilized at the 1−4 positions, and different target DNA samples were applied onto the B−D positions. Hybridization buffer without DNA sample was applied onto the A position as a negative control. The asterisks at positions B1, B2, C1, C3, D1, and D4 represent the positions of perfect match sequences of the normal and corresponding mutant probe DNAs with hybridization of each heterozygous CD sample.

stronger as the length of the target DNA increased to 147-mer. However, it decreased with a further increase of the target DNA length. Intermolecular secondary structures of probes and target DNAs can affect the DNA hybridization in the reaction solution. Thus, the predicted secondary structures of the probes and target DNAs were compared. The secondary structure prediction suggested that the binding sites (red circles) of the target DNAs were well exposed to the probe sites up to 147-mer (Figures S2−S6, Supporting Information). However, the binding sites of the longer target DNAs (190- and 225-mer) became hindered by the formation of their own secondary structures (Figures S7−S8, Supporting Information). Thus, it was concluded that the lower hybridization signals obtained with 190- and 225-mer target DNAs were due to the steric hindrance caused by their formation of secondary structures that negatively affect hybridization with the probe DNAs. Furthermore, binding affinities can be altered by the coiling and folding in the DNA tertiary structure, which becomes more complicated as the length of the target DNA increases. Thus, we decided to use 147-mer target DNA showing the highest hybridization signal and reproducible results in the subsequent experiments.

System Validation and Detection Sensitivity. Figure 4 shows the superimposed spectrum profiles obtained from the MG-NPA chip and the extinction peak observed at 540 nm (black line). When 10 μM CD probe DNAs were immobilized on the surface of the MG-NPA chip, we observed an increase in the extinction intensity (red line). Under similar conditions, hybridization reactions between each CD target and probe DNA caused a significant enhancement in the extinction intensity. The analytical range and sensitivity of the MG-NPA chip were determined by measuring different concentrations of each CD target DNA in the range of 1 fM to 1 μM. The calibration plots shown in Figure 4 display the dependence of the extinction intensity on the concentration of each CD target DNA. The detection limit of the MG-NPA chip was determined as 1 pM for all CD target DNAs with a wide dynamic linear range between 1 pM and 1 μM for Δextinction. Error bars represent the standard deviation of triplicate measurements (n = 3). The standard deviations of the extinction intensity value were less than 10% in all the measurements using three different chips, which indicated that the MG-NPA chips could be fabricated uniformly and are suitable for the fabrication of devices with similar responses.

Hybridization of the Normal and Homozygous Mutant *BIGH3* PCR Products. The results of hybridization experiments using normal and homozygous ACD, RBCD, and LCD samples are shown in Figure 5. The target DNA samples were prepared by using the cloned DNAs described earlier. The words "homozygous" and "heterozygous" are used to describe the genotypes; homozygous means a genotype consisting of two identical alleles at a given locus, while heterozygous means a genotype consisting of two different alleles at a given locus. Figure 5 shows the results of hybridization stringency tests for each type of probe DNA using each type of homozygous target DNA (HOMO) using the 20-MG-NPA chip. Each probe DNA was immobilized at positions 1−4, and different target DNA samples were applied onto the B−E positions. Hybridization buffer without DNA sample was applied

onto the A position as a negative control. In the case of a perfect match, such as a normal type of probe DNA bound to a normal type of target DNA, ACD probe DNA bound to ACD target DNA, RBCD probe DNA bound to RBCD target DNA, and LCD probe DNA bound to LCD target DNA, only the spot at the positions of the normal probe (B1), ACD probe (C2), RBCD probe (D3), and LCD probe (E4) showed the highest increase in extinction. Thus, the single-base mismatch in the *BIGH3* gene could be successfully discriminated by the label-free LSPR-based biosensor system using the MG-NPA.

Detection of the *BIGH3* Point Mutations in Real Patients' Samples Using the MG-NPA Chip. To verify the true applicability of the MG-NPA chip in a clinical setting, real target samples were amplified from patients' DNAs. Most patients' mutation samples are heterozygous, and thus, samples representing heterozygous ACD, RBCD, and LCD were applied onto the 20-MG-NPA chip. As they are heterozygous samples, each one contains one normal allele and one mutant allele. Thus, it can be expected that normal probe DNA and each mutation probe DNA will show the increase in extinction intensity at the same time with a half intensity difference between the perfect match and the mismatch of the homozygous DNA signal. Figure 6 shows the results of hybridization using three heterozygous samples amplified from patients. As expected, hybridization of the heterozygous CD samples resulted in the increases of the extinction intensities at the positions of the normal and the corresponding mutant probes. Thus, the MG-NPA chip developed in this study allows reliable and convenient diagnosis of the heterozygous CDs in addition to the homozygous CDs as described above.

Using the same principles, the MG-NPA chip should be useful for the detection of point mutations prevalent in various genetic diseases and thus would serve as a general platform for the label-free detection of DNA mutations on a chip. Furthermore, this platform represents a novel approach to perform multiplex diagnostics while employing a simple and cost-effective optical setup with disposable chips. Also, effort is being exerted to develop an on-chip microfluidics-integrated MG-NPA system for high-throughput analytical applications.

CONCLUSIONS

A label-free LSPR-based MG-NPA chip was developed and used for the detection of DNA point mutations in the *BIGH3* gene causing CDs. This MG-NPA chip could successfully detect homozygous and heterozygous mutations causing ACD, RBCD, and LCD. This is the first example of detecting DNA point mutations and diagnosing genetic disease using the LSPR-based MG-NPA chip. The MG-NPA chip is easy and inexpensive to fabricate, and the whole diagnostic procedure is simple. Thus, the MG-NPA platform described in this study would be useful as a new diagnostic platform that allows selective and sensitive detection of various DNA point mutations.

ACKNOWLEDGMENT

This research was supported by Avellino (DNA mutation study part) and by the IT Leading R&D Support Project from the Ministry of Knowledge Economy through KEIT (chip part). It was also supported by the World Class University program from the Ministry of Education, Science and Technology through the Korea Science and Engineering Foundation (Grant R32-2008-000-10142-0). Further support by the LG Chem Chair Professorship is appreciated. The first three authors contributed equally to this work.

SUPPORTING INFORMATION AVAILABLE

Additional information as noted in text. This material is available free of charge via the Internet at http://pubs.acs.org.

Received for review October 24, 2009. Accepted January 3, 2010.

AC902410Z